

The role of the N/Z -ratio in colliding nuclei during the fusion of sulfur and lead

Bakhodir Kayumov

Institute of Nuclear Physics
Academy of Science, Uzbekistan

New aspects of the Hadron and Astro/Nuclear Physics.
National University of Uzbekistan, Tashkent.
November 7, 2018

A.K. Nasirov^{1,2}, B.M. Kayumov², G. Mandaglio^{3,4}, G. Giardina⁵, K. Kim⁶,
Y. Kim⁶

- 1 BLTP, Joint Institute for Nuclear Research, Joliot-Curie 6, 141980 Dubna, Russia,
- 2 Institute of Nuclear Physics, Ulugbek, 100214, Tashkent, Uzbekistan,
- 3 Dipartimento di Scienze Chimiche, Biologiche, Farmaceutiche ed Ambientali, University of Messina, Messina, Italy,
- 4 INFN Sezione di Catania, Catania, Italy,
- 5 Dipartimento di Scienze Matematiche e Informatiche, Scienze Fisiche e Scienze della Terra, University of Messina, Messina, Italy,
- 6 Rare Isotope Science Project, Institute for Basic Science, Daejeon 305-811, Republic of Korea.

Table of contents

- 1 Introduction
- 2 Dinuclear system model
- 3 Comparison of $^{34}\text{S}+^{208}\text{Pb}$ and $^{36}\text{S}+^{206}\text{Pb}$ reactions products
- 4 Total cross section of reactions
- 5 Conclusion

Purpose of the work¹

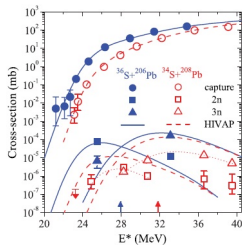
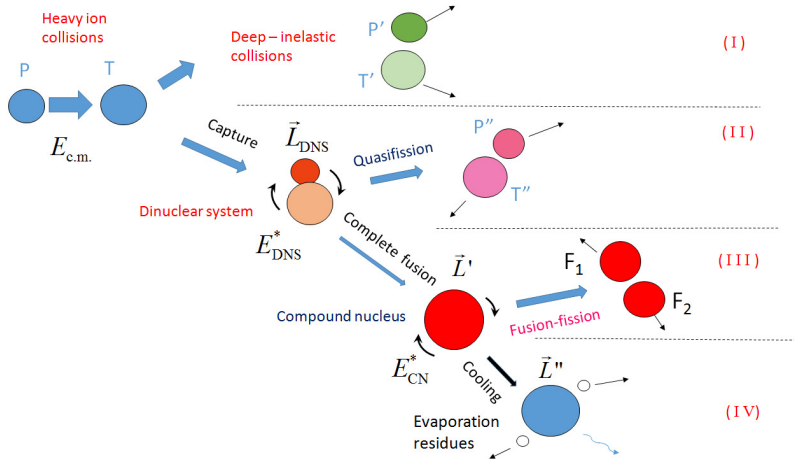


FIG. 3. (Color online) Comparison of capture and ER cross sections as function of the excitation energy of the reactions $^{36}\text{S} + ^{206}\text{Pb}$ (filled symbols, solid lines) and $^{34}\text{S} + ^{208}\text{Pb}$ (open symbols, dashed lines), both forming the same compound nucleus ^{242}Cf . The downward arrow marks an upper cross-section limit, upward arrows mark the positions of the interaction barriers. Solid and dashed lines represent the results HIVAP calculations [15] for the ER cross sections using as input the capture cross sections the results of the coupled-channels calculation. Whereas the ER cross sections of the reaction $^{36}\text{S} + ^{206}\text{Pb}$ are well reproduced, the data of the reaction $^{34}\text{S} + ^{208}\text{Pb}$ (connected by the dotted line to guide the eye) are overestimated.

TABLE III. Experimental and calculated (HIVAP) ER cross sections of the reactions $^{36}\text{S} + ^{206}\text{Pb}$ [5] and $^{34}\text{S} + ^{208}\text{Pb}$ [6] (see also Fig. 3).

Reaction	E^* (MeV)	Evap chan	σ_{exp} (nb)	σ_{cal} (nb)	$\sigma_{\text{exp}}/\sigma_{\text{cal}}$
$^{36}\text{S} + ^{206}\text{Pb}$	25.5	2n	76 ± 10	65	1.2
		3n	7_{-4}^{+6}	1.0	7.0
	33.1	2n	12_{-4}^{+5}	3.0	4.0
		3n	165 ± 20	220	0.75
$^{34}\text{S} + ^{208}\text{Pb}$	24.9	2n	$0.5_{-0.3}^{+0.7}$	5.3	0.09
		2n	$3.0_{-0.5}^{+0.8}$	10	0.30
	3n	$1.7_{-0.5}^{+1.2}$	16	0.11	
	30.7	2n	$1.0_{-0.3}^{+0.5}$	5.0	0.20
		3n	7_{-2}^{+4}	88	0.08
	36.6	2n	$0.7_{-0.5}^{+1.2}$	0.2	3.5
		3n	14_{-2}^{+3}	66	0.21
	39.5	2n	$0.3_{-0.2}^{+1.0}$	<0.1	>3
3n		5_{-1}^{+2}	18	0.28	

¹J. Khuyagbaatar, K. Nishio, S. Hofmann, D. Ackermann, M. Block, S. Heinz, F. P. Heßberger, K. Hirose, H. Ikezoe, B. Kindler, B. Lommel, H. Makii, S. Mitsuoka, I. Nishinaka, T. Ohtsuki, Y. Wakabayashi, and S. Yan, Phys. Rev. C **86**, 064602 (2012)



The sketch of the damped reaction channels

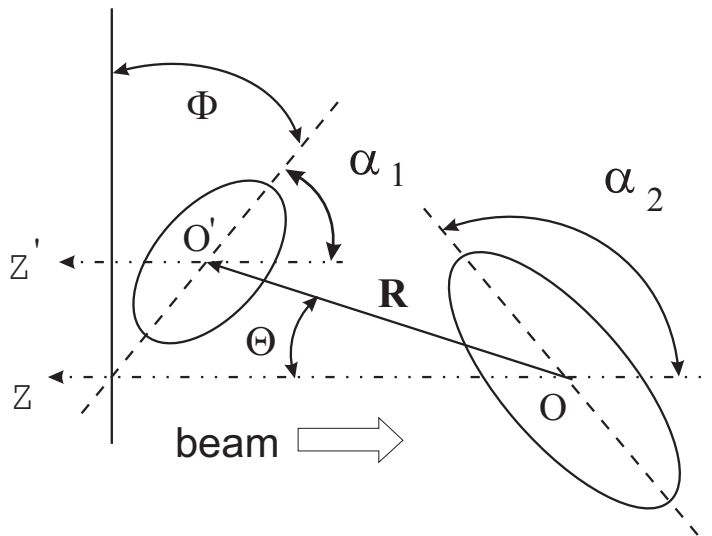
Potential energy

Nucleus–nucleus potential

$$V(R) = V_C(R) + V_N(R) + V_{rot}(R) \quad (1)$$

$$V_C(R) = \frac{Z_1 Z_2}{R} e^2 + \frac{Z_1 Z_2}{R^3} e^2 \left\{ \left(\frac{9}{20\pi} \right)^{1/2} \sum_{i=1}^2 R_{0i}^2 \beta_2^{(i)} P_2(\cos \alpha'_i) + \frac{3}{7\pi} \sum_{i=1}^2 R_{0i}^2 \left[\beta_2^{(i)} P_2(\cos \alpha'_i) \right]^2 \right\}$$

$$V_{rot}(R) = \hbar^2 \frac{l(l+1)}{2\mu R^2}$$



The nuclear part of the nucleus-nucleus potential

$$V_{nucl}(R) = \int \rho_1^{(0)}(\mathbf{r} - \mathbf{R}) f_{eff}[\rho] \rho_2^{(0)}(\mathbf{r}) d^3\mathbf{r},$$

$$f_{eff}[\rho] = C_0 \left(f_{in} + (f_{ex} - f_{in}) \frac{\rho(0) - \rho(r)}{\rho(0)} \right) \quad (2)$$

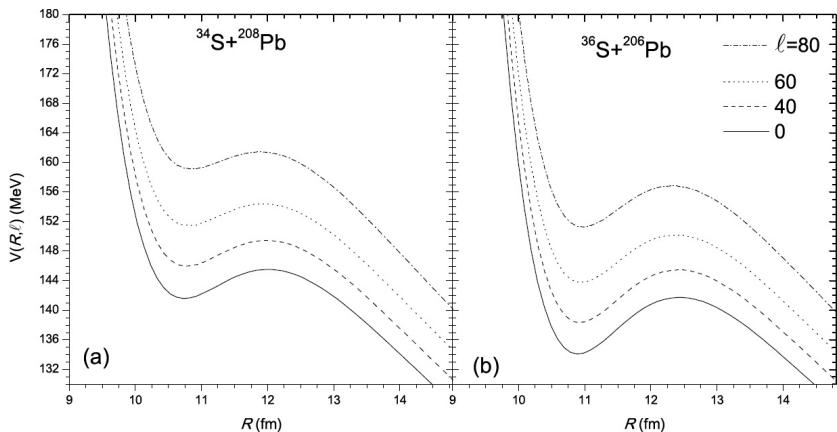
Here $C_0=300 \text{ MeV fm}^3$, $f_{in} = 0.09$, $f_{ex} = -2.59$ are the constants of the effective nucleon-nucleon interaction²; $\rho = \rho_1^{(0)} + \rho_2^{(0)}$.

$$\rho_i^{(0)}(r) = \rho_0 \left\{ 1 + \exp \left[\frac{r - \tilde{R}_i(\beta_2^{(i)}, \beta_3^{(i)}; \theta_i)}{a_0} \right] \right\}^{-1},$$

$$\tilde{R}_i(\beta_2^{(i)}, \beta_3^{(i)}; \theta_i) = R_0^{(i)} \left(1 + \beta_2^{(i)} Y_{20}(\theta_i) + \beta_3^{(i)} Y_{30}(\theta_i') \right),$$

$$\rho_0 = 0.17 \text{ fm}^{-3}, a_0 = 0.54 \text{ fm} \text{ and } i = 1, 2.$$

²A.B. Migdal, *Theory of the Finite Fermi-Systems and Properties of Atomic Nuclei*, Moscow, Nauka (1983).



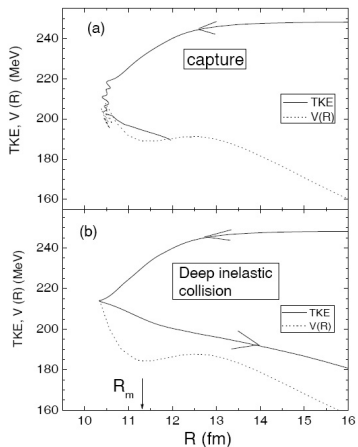
The influences of the rotational angular momentum on nucleus-nucleus potential; for $\alpha_P = 45^\circ$ and $\alpha_T = 30^\circ$ solid line $l = 0$, dashed line $l = 40$, dotted line $l = 60$, dash-dotted line $l = 80$.

Relative motion

Equations of motion

$$\begin{aligned} \mu(R) \frac{d\dot{R}}{dt} + \gamma_R(R) \dot{R}(t) &= F(R), \\ F(R, \alpha_1, \alpha_2) &= -\frac{\partial V(R, \alpha_1, \alpha_2)}{\partial R} - \dot{R}^2 \frac{\partial \mu(R)}{\partial R} \\ \frac{dL}{dt} &= \gamma_\theta(R) R(t) \left(\dot{\theta} R(t) - \dot{\theta}_1 R_{1eff} - \dot{\theta}_2 R_{2eff} \right) \quad (3) \\ L_0 &= J_R(R, \alpha_1, \alpha_2) \dot{\theta} + J_1 \dot{\theta}_1 + J_2 \dot{\theta}_2 \\ E_{rot} &= \frac{J_R(R, \alpha_1, \alpha_2) \dot{\theta}^2}{2} + \frac{J_1 \dot{\theta}_1^2}{2} + \frac{J_2 \dot{\theta}_2^2}{2}. \end{aligned}$$

Relative motion



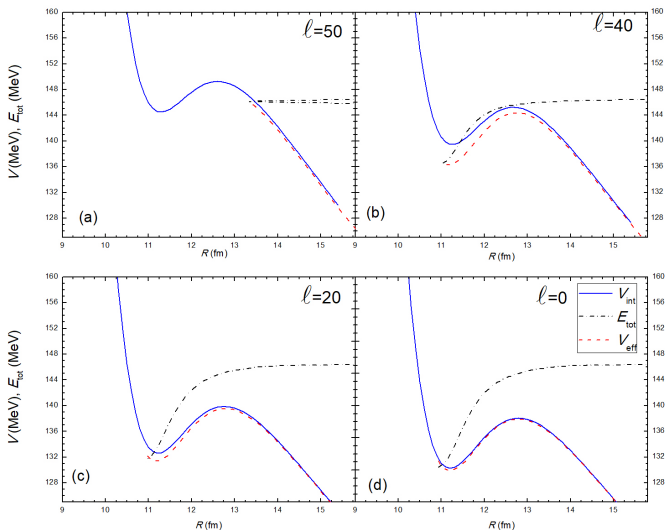
The difference between capture (a) and deep-inelastic collisions (b) caused by the dependence of the dissipation of the total kinetic energy (TKE) of the relative motion and the nucleus-nucleus potential on the radial distance.

Relative motion

Capture cross section

$$\sigma_{cap}^{(\ell)}(E_{c.m.}, \{\alpha_i\}) = \frac{\lambda^2}{4\pi} \mathcal{P}_{cap}^{(\ell)}(E_{c.m.}, \{\alpha_i\}); \quad (4)$$

Our model allows to calculate capture and deep-inelastic collisions of two heavy-ions at the near Coulomb barrier energies. Initial physical quantities are $Z_P, A_P, Z_T, A_T, E_{c.m.}, L, \alpha_1, \alpha_2$.



Deep inelastic collision (a) and capture (b),(c),(d) trajectories at collision energy $E_{\text{c.m.}} = 146.41$ MeV for the $^{36}\text{S} + ^{206}\text{Pb}$ reaction. Blue solid lines are V_{int} ; black dotted lines are E_{tot} ; red dashed lines V_{eff} .

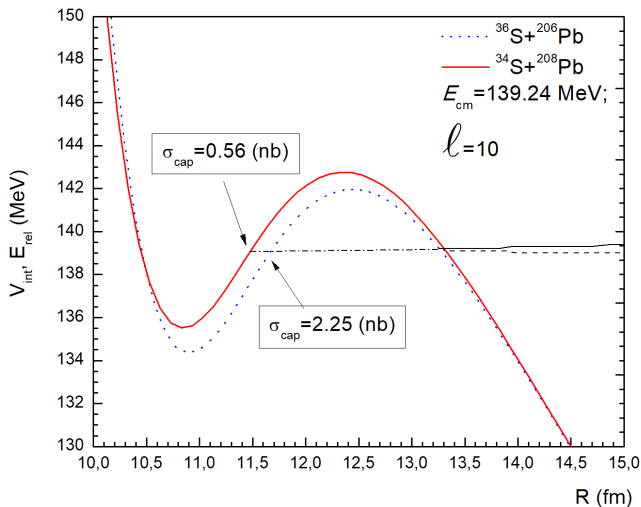
Sub-barrier capture stage

To investigate sub-barrier fusion process where excitation energy is less than 30 MeV:

$$\begin{aligned}
 P(E_{cm}, \ell) &= \int_{R_{in}}^{R_{out}} \sqrt{\frac{2\mu}{\hbar}} (V(R) - E_{cm}) dt; \\
 T(E_{cm}, \ell) &= \exp[-P(E_{cm}, \ell)]; \\
 \sigma(E_{cm}, \ell) &= \frac{\pi \hbar^2}{2\mu E_{cm}} (2\ell + 1) T(E_{cm}, \ell).
 \end{aligned} \tag{5}$$

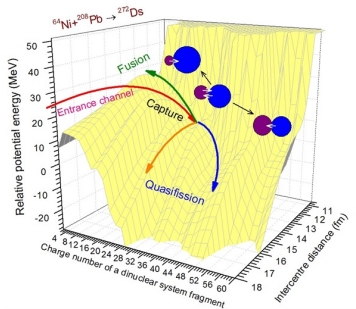
Where $P(E_{cm}, \ell)$ —action integral; $T(E_{cm}, \ell)$ —transmission coefficient; $\sigma(E_{cm}, \ell)$ —partial fusion cross section.

Sub-barrier capture.

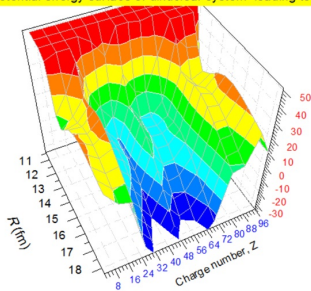


Potential energy surface

$$U(Z, A, R) = B_1(Z, A) + B_2(Z_{CN} - Z, A_{CN} - A) - B_{CN} + V(Z, A, R)$$

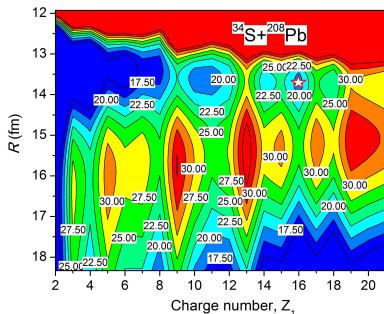
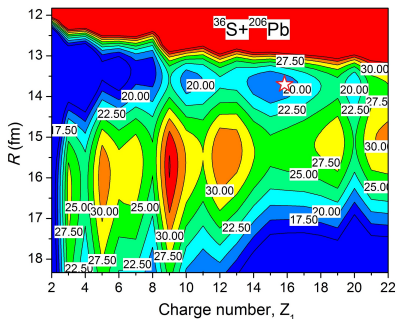


Potential energy surface of dinuclear system leading to ²⁴²Cf



Potential energy surface of the dinuclear system leading to *242Cf

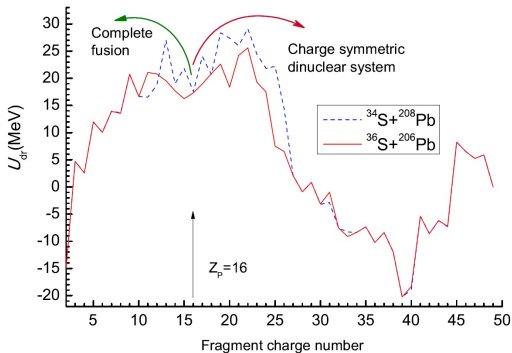
Potential energy surface



Contour maps of the PES calculated for the $^{36}\text{S}+^{206}\text{Pb}$ and $^{34}\text{S}+^{208}\text{Pb}$ reaction with the non-equilibrium distribution of neutrons between the DNS fragments.

Driving potential which is leading ^{242}Cf

$$U(Z, A, R_{min}, \ell) = B_1(Z, A) + B_2(Z, A) - B_{\text{CN}} + V(Z, A, R_{min}, \ell)$$



Charge and mass distributions of the DNS products

The yield of decay fragments

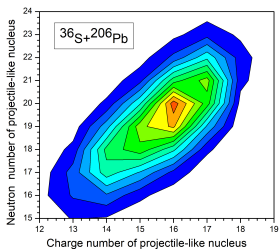
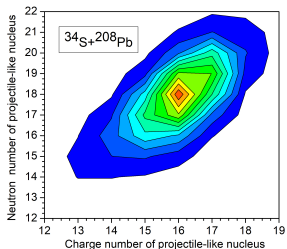
The probability Y_Z of formation of the reaction products with the charge number Z is found by expression

$$Y_K(E_K^*, \ell, t_{int}) = \int_0^{t_{int}} P_K(E_K^*, \ell, t) \Lambda_K^{qf} dt, \quad (6)$$

here $P_K(E_K^*, \ell, t)$ is the probability of the charge and mass ($K = Z, N$) distribution between nuclei of dinuclear system which is calculated by solving the transport master equation:

$$\begin{aligned} \frac{\partial}{\partial t} P_K(E_K^*, \ell, t) &= \Delta_{K+1}^{(-)} P_{K+1}(E_K^*, \ell, t) \\ &+ \Delta_{K-1}^{(+)} P_{K-1}(E_K^*, \ell, t) \\ &- \left(\Delta_K^{(-)} + \Delta_K^{(+)} + \Lambda_K^{qf} \right) P_K(E_K^*, \ell, t) \end{aligned} \quad (7)$$

Yield of DNS products



Evolution of the N/Z ratio in a fragment of dinuclear system formed in the $^{36}\text{S}+^{206}\text{Pb}$ and $^{34}\text{S}+^{208}\text{Pb}$ reactions.

Calculation of total cross section and yield.

$$\sigma_{fus}^{(\ell)}(E_{CN}^*, \{\alpha_i\}) = P_{CN}(E, \ell, \{\alpha_i\}) \times \sigma_{cap}^{(\ell)}(E_{CN}^*, \{\alpha_i\}); \quad (8)$$

$$P_{CN}(E_Z^*, \ell, \{\alpha_i\}) = \sum_{Z_{sym}}^{Z_{max}} Y_Z(E_{CN}^*) \times P_{CN}^{(Z)}(E_Z^*, \ell, \{\alpha_i\}). \quad (9)$$

APPENDIX A: DEFORMED NUCLEI

The expectation values of the capture and fusion cross sections are obtained by averaging the contributions of collisions with different values of the orientation angle, α , which is the angle of the nucleus relatively to the beam direction at the initial stage of reaction:

$$\langle \sigma_i(E_{c.m.}) \rangle = \int_0^{\pi/2} \sin \alpha \sigma_i(E_{c.m.}; \alpha) d\alpha. \quad (A1)$$

Deformation parameters (see Table I) of the ground quadrupole and octupole states are taken from Ref. [17] of the reacting nuclei in this work while the ones of the first excited first 2^+ and 3^- states are obtained from Refs. [27] and [28], respectively.

APPENDIX B: SURFACE VIBRATION

If a nucleus has spherical shape in its ground state and its first 2^+ excited state is deformed, this excited state was considered as the vibrational state. The surface vibrations are regarded as independent harmonic vibrations and the nuclear radius is considered to be distributed as a Gaussian distribution [29].

$$g(\beta_2, \beta_3) = \exp \left[-\frac{[\sum_{\lambda} \beta_{\lambda} Y_{\lambda 0}^*(\alpha)]^2}{2\sigma_{\beta}^2} \right] (2\pi\sigma_{\beta}^2)^{-1/2}, \quad (B1)$$

where α is the direction of the spherical nucleus. For simplicity, we use $\alpha = 0$.

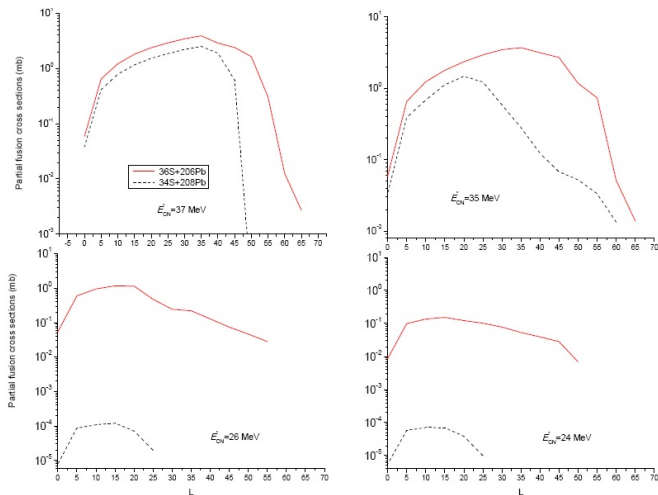
$$\sigma_{\beta}^2 = R_0^2 \sum_{\lambda} \frac{2\lambda + 1}{4\pi} \frac{\hbar}{2D_{\lambda}\omega_{\lambda}} = \frac{R_0^2}{4\pi} \sum_{\lambda} \beta_{\lambda}^2, \quad (B2)$$

$$\langle \sigma_i(E_{c.m.}) \rangle = \int_{-\beta_{2+}}^{\beta_{2+}} \int_{-\beta_{3-}}^{\beta_{3-}} \sigma_i(E_{c.m.}) g(\beta_2, \beta_3) d\beta_2 d\beta_3 \quad (B3)$$

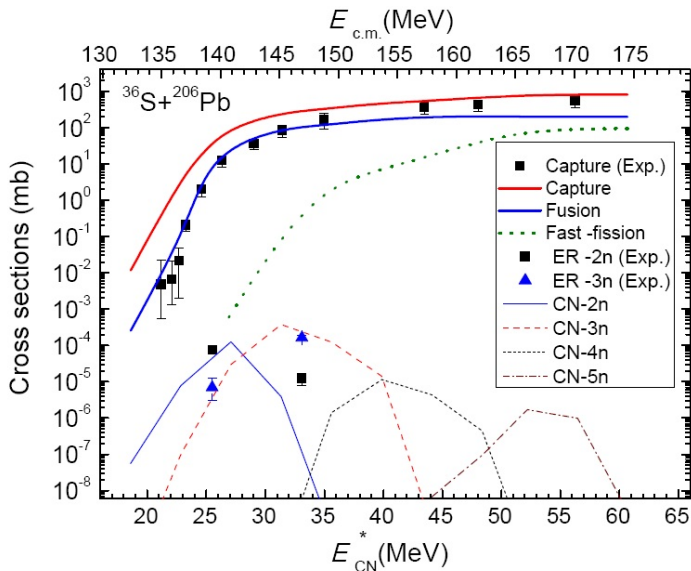
3

³K. Kim, Y. Kim, A.K. Nasirov, G. Mandaglio and G. Giardina Phys. Rev. C **91**, 064608 (2015).

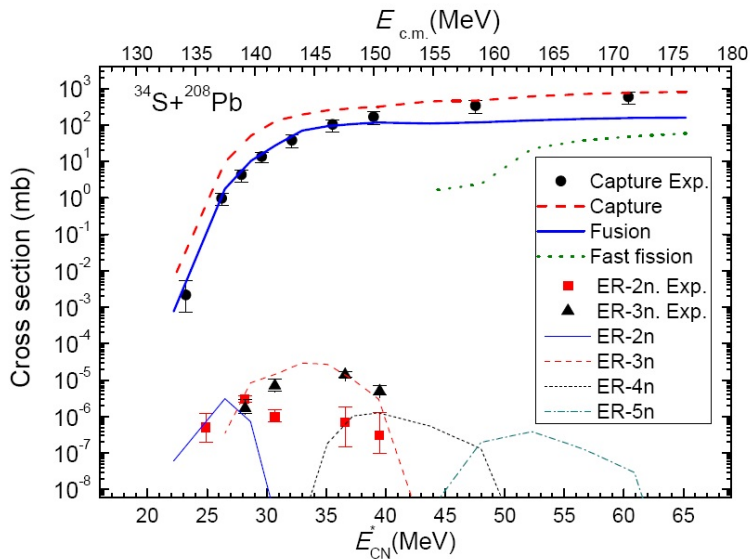
Comparison of partial fusion cross section for $^{36}\text{S}+^{206}\text{Pb}$ and $^{34}\text{S}+^{208}\text{Pb}$.



Comparison of experimental results for $^{36}\text{S}+^{206}\text{Pb}$.



Comparison of experimental results for $^{34}\text{S}+^{208}\text{Pb}$.



- The low barrier of the entrance channel in the $^{36}\text{S}+^{206}\text{Pb}$ reaction is favorable to decrease the CN excitation energy since it makes lower threshold value of the beam energy leading to the CN formation.

- The low barrier of the entrance channel in the $^{36}\text{S}+^{206}\text{Pb}$ reaction is favorable to decrease the CN excitation energy since it makes lower threshold value of the beam energy leading to the CN formation.
- Non-equilibrium stage of the charge and mass distributions between nuclei of DNS at the time $t = 6 \cdot 10^{-22}$ of evolution of DNS is studied to estimate the difference in the fusion probabilities between $^{36}\text{S}+^{206}\text{Pb}$ and $^{34}\text{S}+^{208}\text{Pb}$ reactions.

- The low barrier of the entrance channel in the $^{36}\text{S}+^{206}\text{Pb}$ reaction is favorable to decrease the CN excitation energy since it makes lower threshold value of the beam energy leading to the CN formation.
- Non-equilibrium stage of the charge and mass distributions between nuclei of DNS at the time $t = 6 \cdot 10^{-22}$ of evolution of DNS is studied to estimate the difference in the fusion probabilities between $^{36}\text{S}+^{206}\text{Pb}$ and $^{34}\text{S}+^{208}\text{Pb}$ reactions.
- The difference between the fusion cross sections in these reactions is explained by the higher intrinsic fusion barrier in the $^{34}\text{S}+^{208}\text{Pb}$ reaction. This fact is caused by the distinction of the N/Z -ratios in the light fragments of the DNS formed during the capture in $^{36}\text{S}+^{206}\text{Pb}$ and $^{34}\text{S}+^{208}\text{Pb}$ reactions.

Thanks for attention!

The frequencies ω_m and ω_{qf} are found by:

$$\omega_m^2 = \mu_{qf}^{-1} \left. \frac{\partial^2 V(R)}{\partial R^2} \right|_{R=R_m},$$

$$\omega_{qf}^2 = \mu_{qf}^{-1} \left. \frac{\partial^2 V(R)}{\partial R^2} \right|_{R=R_{qf}}.$$

The calculated values of $\hbar\omega_m$ and $\hbar\omega_{qf}$ were equal to 46.52 MeV and 22.37 MeV, respectively. The collective enhancement factor of the rotational motion K_{rot} is calculated by the well known expression⁴:

$$K_{rot}(E_Z^*) = \begin{cases} (\sigma_{\perp}^2 - 1)f(E_Z^*) + 1, & \text{if } \sigma_{\perp} > 1 \\ 1, & \text{if } \sigma_{\perp} \leq 1, \end{cases}$$

where $\sigma_{\perp} = J_{DNS} T / \hbar^2$; $f(E) = (1 + \exp[(E - E_{cr})/d_{cr}])$; $E_{cr} = 120\tilde{\beta}_2^2 A^{1/3}$ MeV; $d_{cr} = 1400\tilde{\beta}_2^2 A^{2/3}$. $\tilde{\beta}$ is the effective quadrupole deformation for the dinuclear system.

⁴A. R. Junghans, *et al.*, Nucl.Phys. A **629**, 635 (1998)